Aberrations in materials with random inhomogeneities

J. A. Hernández,[a] M. Clark, S. D. Sharples, and M. G. Somekh
School of Elec. and Elec. Engineering, The University of Nottingham, NG7 2RD, United Kingdom

V. H. Lopez
Instituto de Investigaciones Metalúrgicas, UMSNH, Morelia, Mich., México

(Received 20 August 2005; revised 13 December 2006; accepted 13 December 2006)

Materials that consist of a random microstructure can affect ultrasonic measurements—reducing signal strength, increasing noise, and reducing measurement accuracy—through scattering and aberration of the acoustic field. To account for these adverse effects a phase screen model, alongside the stochastic wave equation, has been developed. This approach allows the field and study aberrations to be modeled from a statistical point of view. Experimental evidence of aberration and statistical properties of the measured acoustic field are shown. A measured correlation function of the acoustic field is interlinked to mean crystallite size by using a theoretical coherence function that can be mainly described by the correlation length and wave velocity variation of microstructure. The estimation of the mean crystallite size using this technique would provide some insight into material characterization. © *2007 Acoustical Society of America.* [DOI: 10.1121/1.2431582]

PACS number(s): 43.35.Cg, 43.20.Fn, 43.28.Lv [RLW] Pages: 1396–1405

I. INTRODUCTION

It is well established that the properties of materials are dictated, to a great extent, by their crystallite structure. Crystal refining is a popular practice to enhance or manipulate the properties of materials. For example, in aluminum, a fine equiaxed microstructure leads to benefits such as less shrinkage, reduced porosity, uniform distribution of second phases and obviously improved mechanical properties which are uniform throughout the material. Moreover, it facilitates subsequent processing. To characterize the crystallite structure nondestructive methods are valuable tools to assess the quality of materials and predict mechanical behavior. In this paper the effects of wave-front distortions on ultrasonic surface acoustic wave (SAW) propagation produced by crystallites of polycrystalline materials is studied and used as a means of gathering information about the microstructure itself. The technique is at an early stage and does not provide a means of estimating crystallite size distribution but it does give a measure of mean crystallite size since this can be estimated based on the coherence of the acoustic field. These effects, generally speaking, will be termed ultrasonic aberrations.

There exist in the literature several techniques for measuring the crystallite size. The microstructure itself is assumed to have certain statistical properties, from which it is theoretically possible to calculate the acoustic first moment and in consequence an attenuation coefficient which is proportional to mean crystallite size.[1,2] The mean crystallite size is directly related to a correlation length that defines a random medium that idealizes real microstructure. The energy correlation of the acoustic field is dependent on the correlation length of the medium. So it is indirectly possible to obtain mean crystallite size. A good deal of theoretical and experimental work related to second-order moments and crystallite-noise scattering of acoustic field has been reported.[3–5]

The paper is organized as follows. Section II looks at some aspects of ultrasonic propagation in materials. The theory is based on the stochastic wave equation for random media alongside a phase screen model. This approach allows us to approximate the field in a random medium, therefore propagation of the energy correlation function developed in Sec. III, which is later used for obtaining microstructure characteristics. A set of experiments was performed on three different samples of aluminum, each with a different crystallite size. This experimental work is presented in Sec. IV which describes the experimental procedure (including instrumentation) for collection of the ultrasonic information necessary for statistical analysis of the measured aberrations. In Sec. V the analysis is explained using an estimated transverse energy correlation function of the field. We have also included in this section simulation of acoustic propagation in a random medium to further support the analysis. This measured correlation function is compared in the last section to the modeled function outlined at the beginning of the paper, so that we can check its consistency. It is believed that the technique will be useful for material characterization as it is possible to relate the aberration strength to the mean crystallite size of the material.

II. THEORY

There exist several theoretical approximations of acoustic wave propagation, for both SAW or bulk waves in polycrystalline materials. Some authors have tried to reduce the problem to a scalar description,[6] using integral techniques or even more complicated methods where the first moment is calculated for certain types of linearly elastic solids.[7] In this paper the theoretical description of ultrasound in an inhomogeneous medium is based on the stochastic wave equation in

[a]Electronic mail: eexjah@nottingham.ac.uk

 0001-4966/2007/121(3)/1396/10/$23.00 © 2007 Acoustical Society of America

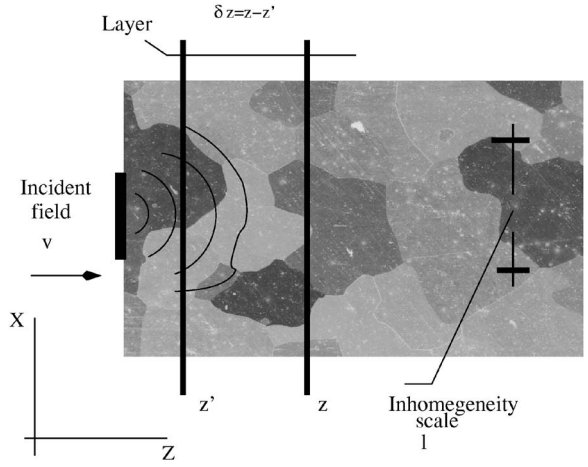

FIG. 1. Schematic representation of ultrasonic propagation in a random medium using phase screen theory.

two dimensions, Eq. (2.1), and a phase screen model widely used in optics and atmospheric calculations.[8,9] Surface acoustic waves in homogeneous materials can be described fairly well by Eq. (2.1).[10,11] It will be seen that this description can be approximately extended to a heterogeneous medium. For that purpose, the ultrasound is assumed to be monochromatic, that is $U(\boldsymbol{r})=u(\boldsymbol{r})e^{-i\omega t}$ which then leads to Helmholtz's equation for u:

$$[\Delta+\bar{k}^2]u(\boldsymbol{r}) \approx -\bar{k}^2\mu(\boldsymbol{r})u(\boldsymbol{r}),$$

$$u(x,0)=v(x), \tag{2.1}$$

where $k^2(\boldsymbol{r})=\bar{k}^2\left(\frac{\bar{c}}{c(\boldsymbol{r})}\right)^2=\bar{k}^2(1+\mu(\boldsymbol{r}))$, μ is a zero mean Gaussian process characterizing the inhomogeneity of the medium, and $\boldsymbol{r}=(x,z)$. The mean velocity $\bar{c}$ here refers to the Rayleigh wave velocity in aluminum. The variance $\sigma^2=\langle(k-\bar{k})^2\rangle/\bar{k}^2$ measures the random fluctuation with respect to the mean wave number $\bar{k}$. The function $v(x)$ is the initial normal displacement, at the plane $z=0$ so Eq. (2.1) would give the normal displacement.

The calculations of first and second moments of Eq. (2.1) has been the subject of several papers. The second-order moments are related to the energy correlation as they coincide under stationary conditions. In this section an approximate representation for the acoustic field is given with the aim of calculating the energy correlation function; this function is similar to the one given in Refs. 12–14, for example. The propagation of v is performed by dividing the space into layers of thickness δz, as shown in Fig. 1, where only half-space is depicted. The acoustic field is then approximated within each layer using equation Eq. (2.1). The thickness δz is taken to be of the order of the correlation length of $k(\boldsymbol{r})$, although the suitability of this choice is not mathematically established in this article.

In order to quantify aberrations or wavefront distortions of the acoustic field, forward scattering only will be considered. This can be done by making the substitution $u=e^{i\bar{k}z}e^{\Phi}$, where Φ is an unknown function to be determined. This leads to parabolic or paraxial approximations of Eq. (2.1) for Φ, which accounts only for forward scattering.[15,16] The function Φ accounts for amplitude and phase variations of the field within a random medium. However, in this article, an alternative method is used to account for amplitude and phase variations of the field u based on a phase screen model. In the general case, Φ is a more complicated function and related to ϕ in Eq. (2.2) but is not discussed in this paper.

The use of a phase screen model to approximate solutions to Eq. (2.1) has long been established.[17–19] The model is stated here with no theoretical analysis but is used to approximate the correlation function of the field. The phase screen model is directly related to solution of the parabolic version of Eq. (2.1) using continual path integrals;[8] this is perhaps the formal justification of this model.

The phase screen model states that if the inhomogeneities do not significantly bend rays with respect to the axis of propagation z, the field within a layer can be approximated by the field in free space and a random screen. This approximation is only valid for weak inhomogeneities or for short path lengths. As a consequence of this approximation the amount of phase change ϕ that an incident field v to a layer of thickness δz would experience is given[8,19,20] by

$$\phi(x)=\frac{\bar{k}}{2}\int_0^{\delta z}\mu(x,z')dz'. \tag{2.2}$$

Thus, the integral in Eq. (2.2) is adding all contributions in phase change that the field would experience along propagation within a layer of thickness δz. This is an approximation since in reality points belonging to wavefront will not follow straight lines, so the integral in Eq. (2.2) will have to be changed to a continual integral.[8]

Let us assume that the screen, which mathematically takes the form of a complex number as $e^{i\phi}$, is located at distance z, which will be the entrance of one layer, then the field behind the screen is given by

$$u(x,z)=v(x)e^{i\phi(x)}. \tag{2.3}$$

The next step is to propagate u in free space to the exit of the layer, which is from z to $z+\delta z$ and is given by Eq. (2.1) with $\mu=0$ and initial condition $u(x,z)$. It is well known that the solution to that problem is given by a plane wave expansion,[21] which is presented below. It has been assumed, in writing Eq. (2.3) that entrance of the layer is located at an arbitrary point $z\neq 0$, thus the limits of integration in Eq. (2.2) should be from z to $z+\delta z$. For simplicity let us assume that the screen is located at $z=0$ then the initial field will be $u(x,0)=v$.

Equation (2.3) indicates that the forward field, at the exit of the layer, is equivalent to the background field phase shifted by ϕ. If the screen is in the middle of the layer, v is propagated to $\frac{\delta z}{2}$ in free space, phase shifted by $e^{i\phi}$, Eq. (2.3) and then free space propagation is again applied up to δz. The propagation and the phase shifting is performed in the spatial frequency domain. So if $\hat{v}(p)$ denotes the Fourier transform of $v(x)$ with respect to x, the solution to Eq. (2.1) with $\mu=0$ is given by[21]

$$u_{\text{free}}\left(x,\frac{\delta z}{2}\right)=\int_{-\infty}^{\infty}\hat{v}(p)h\left(p,\frac{\delta z}{2}\right)e^{ipx}dp, \tag{2.4}$$

where $h(p,z)=\exp\left[iz\bar{k}\left(1-\frac{p^2}{2\bar{k}^2}\right)\right]$ and p is a variable denoting spatial frequency. We are temporally denoting the field u in free space by u_{free} to differentiate it from the one in Eq. (2.5) in a random layer. Taking the Fourier transform of Eq. (2.3) with respect to the variable x and using Eq. (2.4), and reverting back again to the spatial domain by performing the inverse transform gives the representation of u in a random layer as follows:

$$u=\int_{-\infty}^{\infty}\left[\hat{v}(p)h\left(p,\frac{\delta z}{2}\right)\otimes\hat{s}(p)\right]h\left(p,\frac{\delta z}{2}\right)e^{ipx}dp. \tag{2.5}$$

Here $\otimes$ is the convolution operator of two functions and $\hat{v}$, $\hat{s}$ denote the Fourier transform of v, $s=e^{i\phi}$, respectively. Notice, that u in (2.4) and (2.5) is written in the paraxial version by making the approximation $\sqrt{\bar{k}^2-p^2}\approx\bar{k}\left(1-\frac{p^2}{2\bar{k}^2}\right)$, which comes from an exact solution to Helmholtz equation in free space.[21] This approximation is used with the calculations on the correlation function since integrals involving quadratic terms can be performed under suitable conditions. A special case of Eq. (2.5) is $\phi=0$, which results in Eq. (2.4) as expected. Equation (2.5) represents the ultrasound propagating through an inhomogeneous layer which has been approximated by distorting the phase of its elementary components by ϕ.

To extend the propagation to larger propagation distances than δz, Eq. (2.5) is applied recursively to an arbitrary number of layers. So, for instance, since δz is the thickness, u_n indicates the field at $z=n\delta z$ away from source, where $n=1,\ldots,N$, and N is the number of screens within 0 to $z=N\delta z$. Replacing u_n for v and using p_{n+1} instead of p as the dummy variable in expression (2.5) one can see that the field at the exit of the nth layer in the spatial frequency domain is given by

$$\begin{aligned}\hat{u}_{n+1}&=[\hat{u}_n(p_{n+1})h_{p_{n+1}}\otimes\hat{s}(p_{n+1})]h_{p_{n+1}}\\&=h_{p_{n+1}}\int_{-\infty}^{\infty}[\hat{u}_n(p_n)h_{p_n}\hat{s}(p_{n+1}-p_n)]dp_n,\end{aligned} \tag{2.6}$$

where $h_{p_n}=h\left(p_n,\frac{\delta}{2}\right)$ and the convolution operator has been replaced by its definition. Here, also $u_0=v$ as a special case.

Back substitution of the recursive definition for u_n in expression (2.6) shows that the total field $u=u_{n+1}$ at an arbitrary point in space $\boldsymbol{r}=(x,z)$ can then be written as

$$\begin{aligned}u(x,z)=&\int_{-\infty}^{\infty}\cdots\int_{-\infty}^{\infty}\hat{v}(p_0)\prod_{j=0}^{n-1}h_{p_j}^2\hat{s}(p_{j+1}-p_j)\\&\times h_{p_n}e^{ip_nx}dp_0\cdots dp_n.\end{aligned} \tag{2.7}$$

Equation (2.7) represents the ensemble of the acoustic field in a random medium and it will serve as a basis to calculate the energy correlation function. It is a multiple integral and there are as many integrals as there are screens within the slab, however, it is computationally efficient as these can be implemented using the fast Fourier transform (FFT) algorithm. Equation (2.7) represents a SAW traveling in the forward direction in the half-space $(x,0\leq z)$. The above procedure can be applied to propagate the initial displacement v in the other direction by using the symmetry of the Green's function for the Helmholtz equation. The acoustic field is statistically symmetric with respect to axis z, so only half of it will be considered. We have only measured half of the acoustic field in the experimental work, although it is possible to image SAW in both directions.

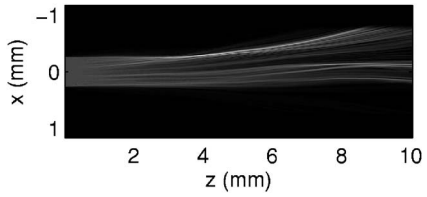

FIG. 2. Amplitude distribution according to Eq. (2.7). The simulation is based on real parameters and a numerical procedure. This can be compared with the experimental amplitude distribution shown in Fig. 6.

The amplitude of a realization numerically implemented from Eq. (2.7) is shown in Fig. 2. It is a truncated acoustic plane wave propagating in simulated inhomogeneous medium characterized by $\sigma=0.02$ according to Eqs. (2.1) and (2.7). As the wave travels from left to right (z direction) the phase is being altered by screens placed to simulate the aberration caused by real microstructure. The overall phase is distorted as well as the amplitude distribution breaking up as it can be seen in Fig. 2. This spread is a typical situation of acoustic surface waves in real experiments. This simulated acoustic field, however, is not expected to follow precisely all wave paths that one would expect to follow in real experiments, such as that shown in Fig. 6. Their similarities are assessed by looking at their statistical properties.

III. PROPAGATION OF ENERGY CORRELATION

The source v can be nonstationary or a wide sense stationary random function. The energy correlation function of a random function is used to measure the strength of aberration and it has the following definition:

$$\Gamma_v(\tau)=\int_{-\infty}^{\infty}v(x)v(x+\tau)dx, \tag{3.1}$$

where $\tau=x-x'$ and x, x' are two arbitrary points in the transverse axis. It is well known that under stationary conditions the average Γ_v is infinite. In this case it is meaningless to consider Eq. (3.1); instead, the power correlation function, $\lim_{X\to\infty}\frac{1}{X}\int_{-X}^{X}v(x)v(x+\tau)dx$ has to be considered. Statistical properties of the medium are crucial in this discussion. Real materials can have very complicated microstructure, so an approximate description is potentially susceptible to large errors. Crystals can in general be considered as randomly distributed spatially with preferred or random orientation, and macroscopically the material can be isotropic or anisotropic. "Randomly distributed" or just "randomly" is being used here as a generic word; so the spatial arrangement of crystallites may follow any probability distribution. Here, for theoretical simplifications

the sample is considered as being composed of randomly oriented scatterers which are either isotropic or weakly anisotropic. This is a restrictive approximation but it appears to be justified as it explains many of the observed phenomena. Another important point is the crystallite shape, which can be described based on the scale length l. This length explicitly describes the form of correlation $\Gamma_k=\langle k(\boldsymbol{r})k(\boldsymbol{r}')\rangle$, which also fully describes μ. A single model is being used which characterizes μ statistically in terms of σ and l. This is a fair representation of metals with equiaxed crystallites whose spatial distribution can be described by an isotropic random process. Complex structures such as an inhomogeneous crystallite size distribution—elongated crystallites—will require a more sophisticated model. Microstructures with elongated crystallites in a preferred direction can experimentally be investigated by propagating ultrasound in multiple directions. The above assumptions can be summarized by saying that μ can be taken to be an isotropic process as a good approximation to describe microstructure for the polycrystal used in the experimental work. Under this condition the correlation function for μ can take any form as long as it is a function through its difference, that is $\Gamma_\mu=\sigma^2 f(|\boldsymbol{r}-\boldsymbol{r}'|)$, f is a suitable function, and $|\boldsymbol{r}-\boldsymbol{r}'|^2=(x-x')^2+(z-z')^2$. In the literature[1,15] the function $\Gamma_\mu=\sigma^2\exp\left[-\frac{|\boldsymbol{r}-\boldsymbol{r}'|^2}{l^2}\right]$ is extensively used and has been shown to be accurate in some applications.[15] Regardless of the geometry for the boundary problem Eq. (2.1), isotropy in both directions is simply establishing that wave velocity variations between grains can be modeled based on a stationary process with exponential correlation in both directions. This is assuming that velocity variations can be measured in a sample big enough or infinite in both directions.

Let us calculate the mean of the squared difference of the phase, that is $\langle[\phi(x)-\phi(x')]^2\rangle$ at two arbitrary points x and x' using relation Eq. (2.2). In doing so by using the exponential form for Γ_μ, the correlation function $C_\phi=\frac{1}{2}\langle[\phi(x)-\phi(x')]^2\rangle$ follows as

$$
\begin{aligned}
C_\phi &= \frac{\bar{k}^2}{4}\int_0^{\delta z}\int_0^{\delta z}\langle[\mu(x,z)-\mu(x',z')]^2\rangle dz dz' \\
&= \frac{\bar{k}^2\sigma^2}{4}[1-e^{-\tau^2/l^2}]\int_0^{\delta z}\int_0^{\delta z} e^{-(z-z')^2/l^2} dz dz' \\
&= \frac{\sqrt{\pi}\bar{k}^2}{4} l\sigma^2\delta z(1-e^{-\tau^2/l^2})\mathrm{erf}\left(\frac{2\delta z}{l}\right),
\end{aligned}
\tag{3.2}
$$

where erf denotes the error function and $\tau=x-x'$. erf can be ignored as a good approximation providing $\delta z\approx l$ or $\delta z\gg l$ which gives $\mathrm{erf}(2\delta z/l)\approx 1$. Under these circumstances the calculation of C_ϕ is equivalent to assume from the very beginning that μ is delta correlated in the z direction or that the correlation of μ takes the form $\Gamma_\mu=\sigma^2\exp[-\tau^2/l^2]\delta(z-z')$. Using this correlation function, the calculation of C_ϕ leads exactly to Eq. (3.2) with $\mathrm{erf}(\frac{2\delta z}{l})$ replaced by 1, which will be used to calculate the correlation function of the field.

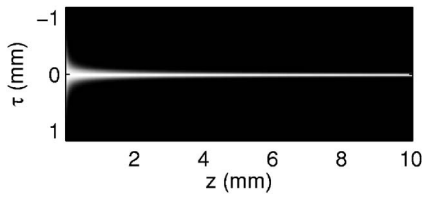

FIG. 3. Image of the energy correlation propagating in a random medium—z direction—with parameters $\sigma=0.02$ and $l=150$ μm, Eq. (3.3).

The energy correlation function of the field is transversally calculated for each propagation distance. Thus, by denoting the correlation function of the field by Γ_u, which is the ensemble average $\langle u(x,z)u^*(x',z)\rangle$ of the field for each propagation distance z, the explicit expression of C_ϕ will allow us to explicitly write Γ_u.

In general, u_n may be statistically related to ϕ for a single layer, because as v propagates from layer to layer u_n depends on ϕ. It will be shown that it is possible, at least mathematically, that the energy correlation of the field can be calculated if the medium is statistically independent of the incident field. Hence, based on those approximations, the expression for the energy correlation function at the entrance and exit of a region are simply related by

$$
\Gamma_u=\Gamma_v(\tau)e^{-NC_\phi}, \tag{3.3}
$$

where C_ϕ is given in Eq. (3.2). An example of the energy correlation over a distance corresponding to several crystallites, as calculated according to Eq. (3.3), is illustrated in Fig. 3. The decay and width as it propagates is determined by σ and l, respectively. The extreme case is for a highly aberrated medium, that is, $\sigma\to 1$ and small l—small crystallites—then Eq. (3.3) decays rapidly having a narrow tail. The ideal case occurs when $\mu=0$, that is homogeneous medium, so Eq. (3.3) does not change with propagation distance.

To show that the last expression is valid in this approximation, Eq. (2.7) will be considered by transforming it to the spatial domain.[21] For that purpose, an independent coordinate is attached for each screen. Therefore, let $\boldsymbol{x}=(x_0,\ldots,x_n)$ be that coordinate system. So if $\phi_0(x_0),\ldots,\phi_n(x_n)$ denotes the phase variation at each screen, then one can define the correlation function at each screen as $C_\phi(x_s,y_s)=\langle[\phi_s(x_s)-\phi_s(y_s)]^2\rangle$. Recall that ϕ is isotropic so C_s is a function of the difference $\tau_s=x_s-y_s$. Let us also consider the product of screen defined as $s(\boldsymbol{x})=e^{i\Sigma_s\phi_s(x_s)}$. Now the Green's function in the paraxial approximation of Eq. (2.1) is given by $g(x-x',z)=\sqrt{\bar{k}/2\pi z}e^{i(\bar{k}/2z)(x-x')^2}$ then the propagator in several variables is simply

$$
G(\boldsymbol{x},z)=\prod_{j=1}^{n} g(x_s^-,z_s^-), \tag{3.4}
$$

where $x_s^-=x_s-x_{s-1}$ and $z_s^-=z_s-z_{s-1}$.

Recall that one wants to calculate the transverse correlation of the field, i.e., $\Gamma_u(x,x',z)=\langle u(x,z)u^*(x',z)\rangle$ at distance z from the source, thus one has to take the ensemble average Eq. (2.7) in the spatial domain. In order to do that let us make $H(\boldsymbol{x},\boldsymbol{y})=G(\boldsymbol{x},z)G^*(\boldsymbol{y},z)$ and define the ensemble av-

erage of vs as $f(\boldsymbol{x},\boldsymbol{y})=\langle v(x_0)v(y_0)\rangle\langle s(\boldsymbol{x})s^*(\boldsymbol{y})\rangle$; the ensemble has been split because v and s are statistically independent. Thus the ensemble average $\langle u(x_n)u^*(y_n)\rangle$ using Eq. (2.7) is given by

$$\Gamma_u=\int_{-\infty}^{\infty}\cdots\int_{-\infty}^{\infty}f(\boldsymbol{x},\boldsymbol{y})H(\boldsymbol{x},\boldsymbol{y})d\boldsymbol{x}d\boldsymbol{y} \tag{3.5}$$

which can be shown to lead to Eq. (3.3). To be able to integrate Eq. (3.5) one would need to calculate the average f but this is not necessary as long as f is a function of the difference $\boldsymbol{x}-\boldsymbol{y}$ only. This is a consequence of ϕ being Gaussian and an isotropic process. Thus, using a standard result in Gaussian multivariate statistics[21] f takes the form

$$f=\langle v(x_0)v(y_0)\rangle e^{-\Sigma_{s=1}^{N}C_\phi(x_s-y_s)}. \tag{3.6}$$

To continue the evaluation of integral Eq. (3.5) more notation is introduced to shorten the length of the equations. Let $\Lambda_s^-=\frac{2(z_{s-1}-z_s)}{\bar{k}}$ and $r_s=(x_s-x_{s-1})^2-(y_s-y_{s-1})^2$ with obvious definition in vectorial form. Then Eq. (3.5) can be rewritten as

$$\Gamma_u=b\int_{-\infty}^{\infty}\cdots\int_{-\infty}^{\infty}f(\boldsymbol{x},\boldsymbol{y})\prod_{s=1}^{N}\left\{\frac{\exp\left[-i\frac{r_s}{\Lambda_s^-}\right]}{\Lambda_s^-}\right\}d\boldsymbol{x}d\boldsymbol{y}, \tag{3.7}$$

where $b=\left(-\frac{1}{\pi}\right)^N$. A further step in calculating the above integral follows by making the following change of variables: $2\boldsymbol{x}=\boldsymbol{p}+\boldsymbol{q}$, $2\boldsymbol{y}=\boldsymbol{q}-\boldsymbol{p}$, therefore $r_s=(p_s-p_{s-1})(q_s-q_{s-1})$ or $r_s=p_s^-q_s^-$. Thus, Γ_u in the new coordinate system is

$$\Gamma_u=b\int_{-\infty}^{\infty}\cdots\int_{-\infty}^{\infty}f(\boldsymbol{p},\boldsymbol{q})\prod_{s=1}^{N}\left\{\frac{\exp\left[-i\frac{p_s^-q_s^-}{\Lambda_s^-}\right]}{\Lambda_s^-}\right\}d\boldsymbol{p}d\boldsymbol{q}. \tag{3.8}$$

Now, using that Eq. (3.6) depends only on the difference of its coordinates, therefore f would be a function of $\boldsymbol{p}$ only, we can perform integration with respect to $\boldsymbol{q}$. Recognizing that the function to be integrated is the Fourier transform of the identity, this results in a product of delta functions. But first, let us express the term appearing inside the exponential function as

$$-i\frac{p_s^-q_s^-}{\Lambda_s^-}=i\sum_s\left[\frac{p_s^-}{\Lambda_s^-}-\frac{p_{s+1}^-}{\Lambda_{s+1}^-}\right] \tag{3.9}$$

with $p_1^-=p_{n+1}^-=0$, since we have added extra terms for convenience. After inserting Eq. (3.9) in Eq. (3.8) and performing integration with respect to $\boldsymbol{q}$, except for the single variable q_0, we have

$$\Gamma_u=\int_{-\infty}^{\infty}f(\boldsymbol{p},q_0)\prod_{s=1}^{N}\Lambda_s^-\delta\left(p_s^--\frac{\Lambda_s^-p_{s+1}^-}{\Lambda_{s+1}^-}\right)\prod_{s=2}^{N}\frac{1}{\Lambda_s^-}d\boldsymbol{p}dq_0, \tag{3.10}$$

where δ is the delta of Dirac. In the above expression N is an even integer otherwise one would have to multiply the term on the right by $(-1)^N$.

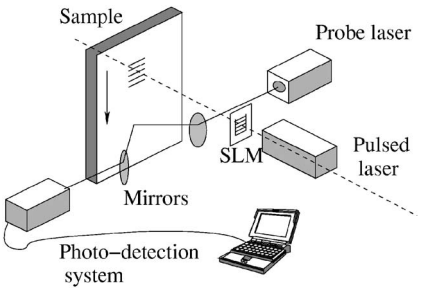

FIG. 4. O-SAM, the optical scanning acoustic microscope. A pattern generated by a spatial light modulator is imaged onto the sample using a pulsed laser. This pattern acts as the source of the surface acoustic waves. The waves are detected by another laser, using the optical beam deflection technique.

Finally integration can be completed by noting that if $\Lambda_s^-=\Lambda_{s+1}^-$ for all s, i.e., all screens are allocated at equal distance in space then we have

$$f(\vec{p_N},q_0)\prod_{s=2}^{N}\Lambda_s^-=\int_{-\infty}^{\infty}f(\boldsymbol{p},q_0)\prod_{s=1}^{N}\Lambda_s^-\delta\left(p_s^--\frac{\Lambda_s^-p_{s+1}^-}{\Lambda_{s+1}^-}\right)d\boldsymbol{p}. \tag{3.11}$$

Here, $\vec{p_N}=(p_N,\ldots,p_N)$. The final expression for Γ_u is obtained by inserting Eqs. (3.6), (3.9), and (3.11) into Eq. (3.10). In doing so

$$\begin{aligned}\Gamma_u&=e^{-NC_\phi(p_N)}\int_{-\infty}^{\infty}\left\langle v\left(\frac{p_N+q_0}{2}\right)v^*\left(\frac{p_N-q_0}{2}\right)\right\rangle dq_0\\&=e^{-NC_\phi(p_N)}\Gamma_v(p_N)\end{aligned} \tag{3.12}$$

which is equivalent to Eq. (3.3) with $p_N=\tau$. The above calculations show that the energy function at distance L is equivalent to the product of individual energy functions at the exit of each layer. Letting N tend to ∞ in Eq. (3.3), Γ_u approximates to a continuous solution of the second-order moment of the Helmholtz's equation. An approximate solution for the second-order moment of Eq. (2.1) is given in Ref. 12 and closely coincides with Γ_u. An expression for the coherence function of the backscattering field is also given in that paper.

IV. MEASUREMENTS

A. The O-SAM instrument

Over the past few years an optical scanning acoustic microscope (O-SAM) has been developed.[22] This highly flexible instrument can be fully automated and is capable of performing multiple acoustic measurements over the surface of a sample. A complete set of software and electronics has been developed for gathering information at high speed. Typically, an amplitude and phase c-scan over an area of 1.5 cm×1.5 cm with a resolution of 10 μm takes a few minutes. Advantage has been taken of these capabilities and the O-SAM was used to build up an ensemble of the acoustic field over the surface of an aberrating material. The main components of O-SAM are shown in Fig. 4. It uses a Q-switched mode-locked Nd-YAG laser for SAW generation, by using a spatial light modulator (SLM) to image any

desirable pattern—typically a set of arcs or straight lines—onto the surface of the material under investigation. This image, illuminated by the pulsed laser, acts as the source of the surface waves. The fundamental frequency at which the O-SAM generates ultrasound is 82 MHz, but multiples of that frequency can also be generated. A second continuous wave laser was used to detect the propagating surface waves using an optical beam deflection technique. Both the detection system and the sample are mounted on computer-controlled automated stages, and so the O-SAM is capable of rapidly imaging the propagating wavefront, at any position on the sample. A more complete overview and technical details are given in Ref. 22.

B. Sample preparation

Three different aluminum samples were created, each with a different mean crystallite size. The procedure is similar for all of them so only a detailed description for one sample is described here. An Al (99.9%) charge of 500 g in mass, contained in a clay bonded SiC crucible, was heated to 730 °C in a muffle furnace. After melting of the Al charge and in order to obtain a lightly refined Al ingot, 0.2 wt. % of an Al-Ti-B commercial crystallite refiner was added and dissolved into the melt. Prior to removal of the oxide skin from the surface of the molten metal, the melt was cast into a rectangular steel mold in which it was allowed to solidify naturally. The Al ingot was released from the mold and sectioned with a band saw. Due to the geometry of the steel mold, a coarse columnar crystallite structure is expected in the top part of the Al ingot. For this reason, that section was removed and four useful blocks were obtained. Owing to the symmetry of the ingot, only three blocks were used; one for the counter part for metallographic characterization and the third was subjected to macro-etching to reveal the overall crystallite structure. Samples for metallography were taken from one block and were mounted, ground and polished down to 1 μm following standard procedures. The same preparation was given to the counter face of the other block. To reveal the crystallite structure, the Al block was repeatedly immersed into a solution (38% H_2O, 45% HCl, 15% HNO_3, and 2% HF) and washed until a good contrast was achieved. Also, the Al-polished samples were anodized in a 2% solution of HBF_4 in water for 1 min at 25 V.[23] After washing and drying, the samples were viewed and imaged in an optical microscope, equipped with a digital camera, under cross-polarized light.

Finally the crystallite size distribution of each of the three samples was determined by applying open source software.[24] Using the software, the perimeter was measured for each region contained within each micrograph and stored in a file for mean estimation. The mean caliper diameter, as defined in Ref. 25, was obtained by dividing the mean diameter of each region by π. The results were approximately as follows: 1345 μm, 785 μm, and 134 μm for A, B, and C, respectively. Also Fig. 5 shows the standard deviation and number of regions considered, σ_i, N_i where $i=A,B,C$, respectively for each block characterized.

Sample A has a more complicated microstructure compared to samples labeled B and C. The latter two have homogeneous distribution of convex crystallites, as can be seen in the micrographs in Fig. 5. On the other hand A has large crystallites of a more complicated form. This feature made samples B and C easy for characterization and ultrasonic analysis, while A was more difficult.

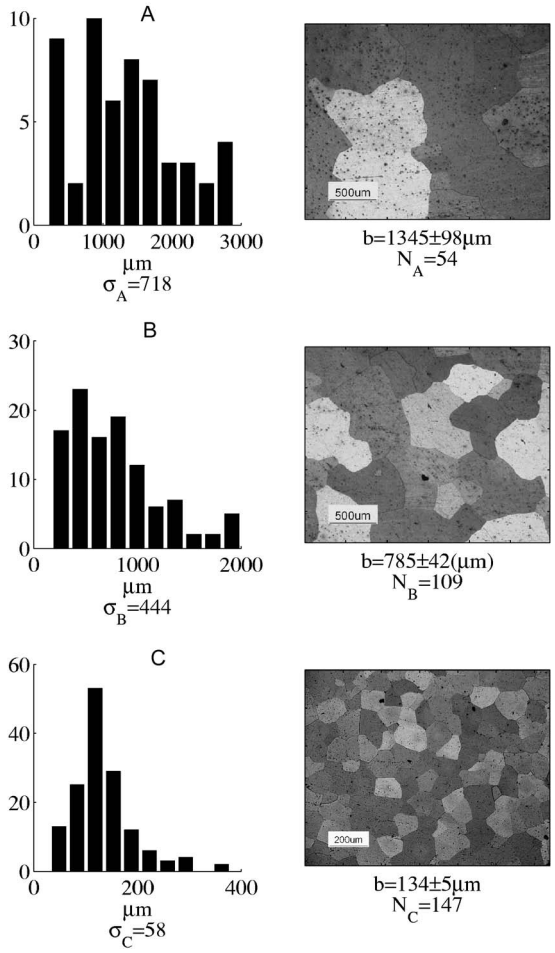

FIG. 5. The first column is the graph for the crystallite size distribution for each micrograph to the right. The second column shows micrographs of aluminum with variations on microstructure.

C. Aberrations in aluminum

Aberrations were investigated in blocks of aluminum of 6 cm × 4 cm × 1 cm, which gives sufficient room for multiple measurements since the scanning area is typically 3 mm × 10 mm. The SLM was programmed to project a series of straight lines onto the surface of the sample, each line separated from its nearest neighbor by a distance equal to the wavelength of the surface waves at 82 MHz, which is the fundamental frequency of the excitation laser. This pattern is used to propagate a plane wave. The propagation resembles a diffraction pattern through a slit since the SLM has finite aperture, so diffraction occurs near the edges. Figure 6 is a typical image of a plane wave propagating from left to right in an inhomogeneous medium. The wavefront breaks up due to aberration caused by the crystallite structure, leading to variations in the amplitude of the wavefront. The statistical analysis of the speckle pattern obtained is expected to pro-

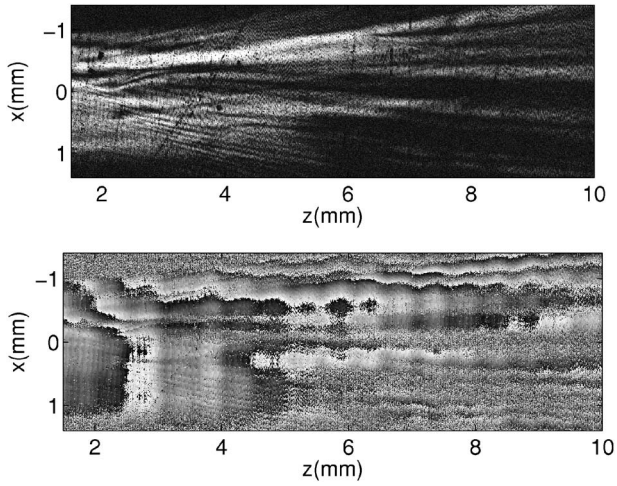

FIG. 6. Amplitude (top) and phase (bottom) of 82 MHz surface acoustic waves, propagating on aluminum. The wavefront breaks up as the ultrasonic wave travels through the crystallites.

vide information about the microstructure. In order to allow the ultrasound to interact with different sets of crystallites the ultrasonic source was positioned at different locations, scanning an area of 3 mm $\times$ 10 mm each time. In this way, approximately 100 pictures similar to those in Fig. 6 were obtained; this was then used to produce an ultrasonic ensemble. All of them are different in detail but are assumed to arise from the same statistical population. Figure 7 is a schematic representation of the procedure used to make multiple measurements. It is important to highlight that the procedure is fully automated so it was only necessary to create a script in order to perform all the measurements.

V. STATISTICAL ANALYSIS

A. Procedure

The discussion is based on statistical concepts such as the second-order moment or energy correlation function for finite sequences. Notation will be introduced to explain some of the concepts and to be able to compare them with the theory earlier developed in Sec. III. Measurements are being denoted by U_{kl}^n as in Fig. 7, so U_{kl}^n represents any of the acoustic ensemble measured on block A, B, and C, where $k=1,\ldots,K$, $l=1,\ldots,L$ and K, L are determined by the resolution of the measured acoustic field in x, z direction, respectively. The superindex $n=1,\ldots,N$ is to indicate the number of field measured on each sample. By definition the cross

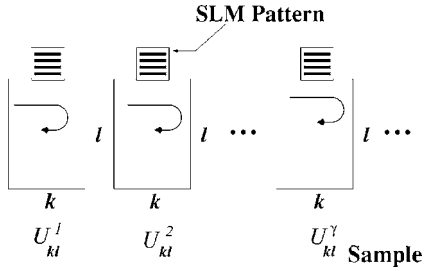

FIG. 7. Schematic representation of scanning area and source locations to build up an ultrasonic ensemble.

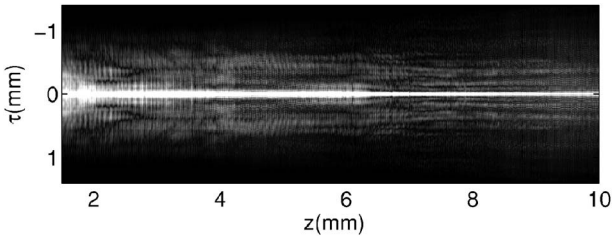

FIG. 8. Measured correlation function according to Eq. (5.2). This is a single instance of Γ_e. Averaging over many instances gives Γ_e which resembles the function in Fig. 3.

correlation is $\langle U_{kl}^n U_{k'l}^{n*}\rangle$ where $\langle\ \rangle$ denotes the ensemble average. The estimation of the ensemble average of $Z_{kk'l}^n = U_{kl}^n U_{k'l}^{n*}$ is rather complicated since there is little statistical information about U_{kl}^n. Instead, two different averages will be performed. By making $m=k-k'$, $Z_{kk'l}$ can be rewritten as $Z_{k,k+m,l}^n = U_k^n U_{k+m,l}^{n*}$. Since there is a waveform for each m, the average over k is performed as well as the ensemble average, leading to

$$Z = \frac{1}{NK}\sum_{n=1}^{N}\sum_{k=1}^{K} Z_{k,k+m,l}^n. \tag{5.1}$$

Z is a complex function so its modulus will be considered, and it will be termed energy correlation or the autocorrelation function; hence,

$$\Gamma_e = \|Z\|. \tag{5.2}$$

The subindex e stands for experimental and is used to differentiate it from the theoretical one. The measured autocorrelation function Γ_e, implemented numerically, is shown in Fig. 8. The importance of this function will become apparent when it is compared to the theoretical Γ_u in Eq. (3.3), since it is related to microstructure. Figure 8 shows that the autocorrelation propagates as an ultrasonic disturbance. The overall decay of this function is strongly related to aberrations due to the interaction between the crystallite structure and the ultrasound. There are two parameters which are free in Eq. (3.3), being σ and l which represents the average crystallite size. An estimation of σ, l has been obtained, for cases A, B, and C by minimizing the following function along propagation distance:

$$\chi^2(\sigma,l) = \sum_{i=1}^{K}\sum_{j=1}^{L}[\Gamma_u(\tau_i,z_i{:}\sigma,l) - \Gamma_e]^2. \tag{5.3}$$

This method of estimating the parameter σ, l proved to be useful only for samples labeled B and C as it will be shown in the last section.

B. Corroboration of model and statistical analysis technique

In Sec. III, Eq. (3.3) linked the theoretical statistical properties of the material microstructure with the autocorrelation function obtained from an ensemble of measured acoustic fields. In order to corroborate the approach of the analysis of this measured data, the phase screen approximation model described in Sec. II was used to simulate a set of

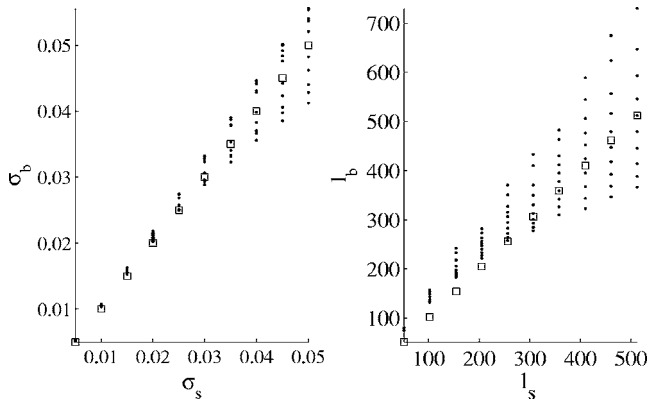

FIG. 9. Subscript s stands for simulation and subscript b for fitted parameters according to Eq. (3.3).

ultrasonic fields propagating through a simulated aberrating medium of known statistical properties. Each of the fields propagated through different simulated crystallite structures, and their corresponding propagating correlation functions were combined into an ensemble average as described by Eq. (5.2). The statistical analysis described in Sec. V A was performed, and the results for standard deviation (σ) and mean crystallite size (l) were compared to the values used to generate the ultrasonic fields. The simulations were repeated for different values of variance and mean crystallite size, and the results are illustrated in Fig. 9. We are using the symbols l_s, σ_s for correlation length and standard deviation used in the simulations, respectively, whereas l_b, σ_b will stand for the best values obtained by minimizing χ^2, Eq. (5.3), for each simulation. In Fig. 9, in the left graph, σ_s is used for the abscissas as well as the ordinate, that is (σ_s,σ_s). In the same box, (σ_s,σ_b) is also being plotted for comparison. So if σ_s and σ_b are the same then the graph will be a straight line. The same principle applies for the graph on the right where we are plotting (l_s,l_s) as well as (l_s,l_b). The small squares in the left graph in Fig. 9 correspond to values of σ_s whereas the squares in the right to l_s. The black dots correspond to σ_b and l_b in the same order as before for each simulation.

One hundred different mediums were simulated by feeding the algorithm with ten values for σ_s and ten for l_s, varying σ_s from 0.01 to 0.05, and l_s from 51 to 512. For each pair (σ_s,l_s), one hundred fields were generated to be able to have a good estimation of average Eq. (5.1). The agreement between the values used to simulate the random microstructure, and the values obtained from statistical analysis of the ensemble autocorrelation functions is good, particularly for the standard deviation. The spread on the estimated crystallite size according to Eq. (5.3) needs more careful analysis since function Eq. (3.3) becomes complicated in that region because σ and l are tightly related, so the algorithm has some difficulties in identifying the right values, particularly so for the correlation length.

It should be remembered that the method used to generate the simulated random crystallite structure and the analysis of the autocorrelation functions are not directly math-

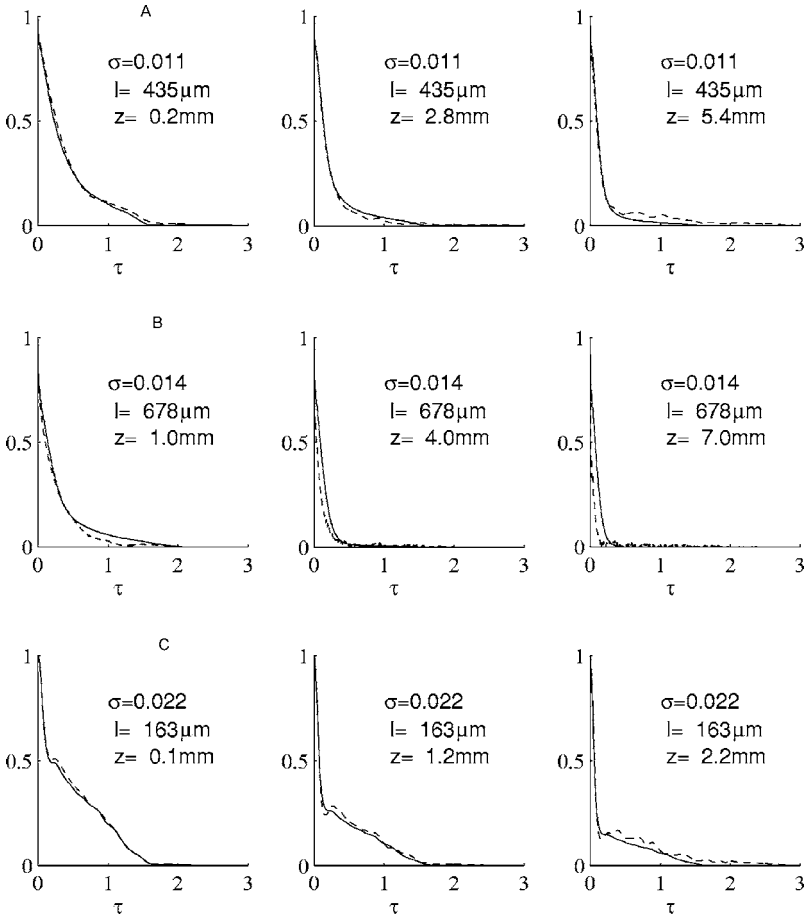

FIG. 10. Comparison of normalized energy correlation functions Γ_u and Γ_e for samples in Fig. 5. The continuous line (—) is derived from Eq. (3.3) at different propagation distances, with values of σ and l shown in each graph. The dashed line (- -) represents the correlation function of the experimental acoustic field at the same propagation distances. The parameters σ and l are within a 20% accuracy.

ematically related. The simulation has been used in a previous paper to study the effects of aberration on wave velocity measurements.[26]

C. Analysis of experimental data

The main result in this section is the comparison between theory and the measured autocorrelation function. The scan area for each picture was taken to be 3 mm wide whereas the propagation distance was chosen until the ultrasonic field became diffuse. In the first case, sample C, the maximum propagation distance was 2.5 mm for instance, using steps of 5 μm in the x axis and 100 μm in the direction of propagation (the z axis). The experimental data acquired by the O-SAM instrument was processed in the same way as the modeled data used at the beginning of this section, and comparisons are made between the measured (Γ_e) and predicted (Γ_u) energy correlation functions at various propagation distances.

Accumulated noise at the central peak of the energy function gives a very sharp peak affecting the overall decay of the energy function, and therefore the estimated values of σ, l. The data were filtered assuming a linear model of the form $y_1=y_2+e$ where e is a white noise statistically uncorrelated to y_1, and y_2 is data free of noise. When filtered with an optimum filter the residual is delta correlated, which corresponds to noise. This can be removed with retention of the desired signal. This very simple model considerably reduces the central peak due to noise, giving the results shown in Fig. 10.

Figure 10 shows the comparison of the measured (Γ_e) and predicted (Γ_u) energy correlation functions—where Γ_u is shown in solid lines—for samples A, B, and C. In each case, it is shown at three different propagation distances in order to illustrate the decay of the correlation function with distance. The dashed lines in Fig. 10 represent the measured energy correlation function on the samples at the same propagation distances, derived from the acoustic ensemble in samples A, B, and C. There is good agreement for samples B and C. The standard deviation which measures the velocity variations from crystallite to crystallite used in Fig. 10, for comparison, is approximately $\sigma \approx 0.015$ which is a value that one would expect for aluminum.[1]

The nonlinear fitting Eq. (5.1), numerically solved, gives the following estimation for σ and l. $[\sigma\ l]=[0.011\ 435\ \mu\text{m}]$, $[\sigma\ l]=[0.014\ 678\ \mu\text{m}]$, and $[\sigma\ l]=[0.022\ 163\ \mu\text{m}]$ for samples A, B, and C, respectively. The estimation of σ is reasonable in all cases, however, the estimated correlation length for sample A is significantly different from the values obtained visually, which are 1345 μm, 785 μm, and 134 μm as shown in Fig. 5.

Possible reasons for this are as follows. First, due to mechanical limitations in the O-SAM instrument, the acoustic field on sample A could not be mapped in its entirety. This effectively truncated the available dataset from which an estimation could be made. Second, we note that the measured mean crystallite size (1345 μm) is approaching the width of the acoustic source ($\approx$2 mm). This is significant, because Γ_e is influenced more by the acoustic aperture in this case than by the correlation length. Finally, as noted in Sec. IV B, the large crystallites in sample A have a complicated form, in that many of the crystallites are nonconvex.

VI. CONCLUSIONS

A theory has been developed to relate statistical parameters of material microstructure to statistics of ultrasonic aberrations. From this relationship it is possible to investigate—indirectly—mean crystallite size and variance of the acoustic wave velocity under certain conditions.

Therefore, the technique as a whole may be used as a tool for material characterization. This technique is particularly suitable for materials that are weakly anisotropic and the crystallite structure is not very complicated. Also, it works well if the width of the source is bigger than the average crystallite size. A phase screen model, alongside the stochastic wave equation, has been developed to simulate ultrasound propagating through random media. This model has been used to corroborate the technique of statistical analysis of the propagating energy correlation function, and provides a useful test bed for developing the theory, alongside the experimental work. The experimental results shown are in good agreement with the analytic expression for the correlation function calculated in Sec. III, provided the conditions discussed in the article are met.

ACKNOWLEDGMENTS

I would like to thank The University of Nottingham for the funding provided, The Engineering and Physical Science Research Council (EPSRC), and the UK center for NDE for supporting this work. We would like also to thank the referees for their helpful and constructive comments.

[1] R. Ranganathan and S. Dattagupta, "Theory of ultrasonic scattering by grains in polycrystals," Phys. Status Solidi A **54**, 537 (1979).
[2] J. Saniie and T. Wang, "Statistical evaluation of backscattered ultrasonic grain signal," J. Acoust. Soc. Am. **84**, 400–408 (1988).
[3] P. Haldipur, F. J. Margetan, L. Yu, R. B. Thompson, and J. A. Turner, "Ultrasonic attenuation measurements in jet-engine nickel alloys," **20**, 1338–1345 (2001).
[4] F. J. Margetan, L. Yu, and R. B. Thompson, "Computation of crystallite-noise scattering coefficients for ultrasonic pitch/catch inspection of metals," Rev. Prog. Quant. Nondestr. Eval. **24**, 1300–1315 (2005).
[5] R. B. Thompson, L. Yu, and F. J. Margetan, "A formal theory for the spatial correlation of backscattered ultrasonic crystallite noise," Rev. Prog. Quant. Nondestr. Eval. **24B**, 1292–1315 (2005).
[6] J. McCoy, "A parabolic theory for stress wave propagation through inhomogeneous linearly elastic solids," J. Appl. Mech. **44**, 462–468 (1977).
[7] M. J. Beran and J. McCoy, "Mean field variations in a statistical sample of heterogeneous linearly elastic solid," **6**, 1035–1054 (1970).
[8] V. U. Zavorotnyi, V. I. Klyatskin, and V. I. Tatarskii, "Strong fluctuations of the intensity of electromagnetic waves in randomly inhomogeneous media," Sov. Phys. JETP **46**, 252 (1977).
[9] J. W. Goodman, *Statistical Optics* (Wiley, New York, 2000).
[10] K. F. Graff, *Wave Motion in Elastic Waves* (Ely House, London, 1975).
[11] L. Rose, "Point-source representation for laser-generated ultrasound," J. Acoust. Soc. Am. **75**, 723–732 (1984).
[12] D. A. de Wolf, "Backscatter corrections to the parabolic wave equations," J. Opt. Soc. Am. **6**, 174–179 (1989).
[13] V. E. Ostashev and V. I. Tatarskii, "Representation of the Helmholtz equation solution in the form of a series based on backscattering multiplicity," Waves Random Media **5**, 125–135 (1995).
[14] C. L. Rino, "On propagation in continuous random media," Waves Random Media **2**, 59–72 (1991).
[15] A. Ishimaru, *Wave Propagation and Scattering in Random Media* (Aca-

demic, New York, 1970).
[16]K. Sobczyk, *Stochastic Wave Propagation* (PWN-Polish Scientific Publishers, Warsaw, 1984).
[17]M. D. Feit and J. J. A. Fleck, "Light propagation in graded-index optical fibers," Appl. Opt. **17**, 3990–3997 (1978).
[18]J. M. Martin and S. M. Flatté, "Intensity images and statistics from numerical simulation of wave propagation in 3-d random media," Appl. Opt. **27**, 2111–2125 (1988).
[19]D. J. Thomson, "A wide-angle split-step algorithm for the parabolic equation," J. Acoust. Soc. Am. **74**, 1848–1854 (1983).
[20]J. A. Neubert, "Asymptotic solution of the stochastic Helmholtz equation for turbulent water," J. Acoust. Soc. Am. **48**, 1203–1211 (1970).
[21]L. Mandel and E. Wolf, *Optical Coherence and Quantum Optics* (Cambridge University Press, Cambridge, 1995).
[22]S. D. Sharples, M. Clark, and M. G. Somekh, "All-optical adaptive scanning acoustic microscope," Ultrasonics **41**, 295–299 (2003).
[23]V. H. Lopez, S. Truelove, and A. Kennedy, "Fabrication of Al-TiC master composites and their dispersion in Al, Cu and Mg melts," Mater. Sci. Technol. **19**, 925–930 (2003).
[24]ImageJ: http://rsb.info.nih.gov/ij/. Last viewed 2/7/07.
[25]J. Ohser and F. M, *Statistical Analysis of Microstructure in Materials Science* (Wiley, New York, 2000).
[26]M. Clark, S. D. Sharples, and M. G. Somekh, "Optimization using measured Green's function for improving spatial coherence in acoustic measurements," Ultrasonics **42**, 205–212 (2004).